Video Article

Probing and Mapping Electrode Surfaces in Solid Oxide Fuel Cells

Kevin S. Blinn[1], Xiaxi Li[1], Mingfei Liu[1], Lawrence A. Bottomley[2], Meilin Liu[1]

[1]Center for Innovative Fuel Cells and Battery Technologies, School of Materials Science and Engineering, Georgia Institute of Technology

[2]School of Chemistry and Biochemistry, Georgia Institute of Technology

Correspondence to: Meilin Liu at meilin.liu@mse.gatech.edu

URL: https://www.jove.com/video/50161
DOI: doi:10.3791/50161

Keywords: Materials Science, Issue 67, Chemistry, Electrical Engineering, Physics, electrochemistry, catalysts (chemical), spectroscopic chemical analysis (application), microscopes, Fuel cell, Raman, AFM, SOFC, Surface, Electrode

Date Published: 9/20/2012

Citation: Blinn, K.S., Li, X., Liu, M., Bottomley, L.A., Liu, M. Probing and Mapping Electrode Surfaces in Solid Oxide Fuel Cells. *J. Vis. Exp.* (67), e50161, doi:10.3791/50161 (2012).

Abstract

Solid oxide fuel cells (SOFCs) are potentially the most efficient and cost-effective solution to utilization of a wide variety of fuels beyond hydrogen [1-7]. The performance of SOFCs and the rates of many chemical and energy transformation processes in energy storage and conversion devices in general are limited primarily by charge and mass transfer along electrode surfaces and across interfaces. Unfortunately, the mechanistic understanding of these processes is still lacking, due largely to the difficulty of characterizing these processes under *in situ* conditions. This knowledge gap is a chief obstacle to SOFC commercialization. The development of tools for probing and mapping surface chemistries relevant to electrode reactions is vital to unraveling the mechanisms of surface processes and to achieving rational design of new electrode materials for more efficient energy storage and conversion[2]. Among the relatively few *in situ* surface analysis methods, Raman spectroscopy can be performed even with high temperatures and harsh atmospheres, making it ideal for characterizing chemical processes relevant to SOFC anode performance and degradation[8-12]. It can also be used alongside electrochemical measurements, potentially allowing direct correlation of electrochemistry to surface chemistry in an operating cell. Proper *in situ* Raman mapping measurements would be useful for pin-pointing important anode reaction mechanisms because of its sensitivity to the relevant species, including anode performance degradation through carbon deposition[8, 10, 13, 14] ("coking") and sulfur poisoning[11, 15] and the manner in which surface modifications stave off this degradation[16]. The current work demonstrates significant progress towards this capability. In addition, the family of scanning probe microscopy (SPM) techniques provides a special approach to interrogate the electrode surface with nanoscale resolution. Besides the surface topography that is routinely collected by AFM and STM, other properties such as local electronic states, ion diffusion coefficient and surface potential can also be investigated[17-22]. In this work, electrochemical measurements, Raman spectroscopy, and SPM were used in conjunction with a novel test electrode platform that consists of a Ni mesh electrode embedded in an yttria-stabilized zirconia (YSZ) electrolyte. Cell performance testing and impedance spectroscopy under fuel containing H_2S was characterized, and Raman mapping was used to further elucidate the nature of sulfur poisoning. *In situ* Raman monitoring was used to investigate coking behavior. Finally, atomic force microscopy (AFM) and electrostatic force microscopy (EFM) were used to further visualize carbon deposition on the nanoscale. From this research, we desire to produce a more complete picture of the SOFC anode.

Video Link

The video component of this article can be found at https://www.jove.com/video/50161/

Protocol

1. Fabrication of a YSZ-embedded Mesh Anode Cell

1. Weigh out two batches of 0.2 g of YSZ powder.
2. Compress one batch YSZ powder in a cylindrical stainless steel mold (13 mm in diameter) with a uniaxial dry press at a pressure of 50 MPa for 30 sec.
3. Cut a <1-cm piece of Ni mesh and place it onto the surface of YSZ disc inside the mold.
4. Add the other 0.2 g of YSZ powder on top of the Ni-mesh inside the mold and flatten the surface of the powder using a ram.
5. Uniaxially press the Ni mesh sandwiched between packs of YSZ powder at a pressure of 300 MPa for 30 sec.
6. Extract the pressed Ni/YSZ pellet from the mold.
7. Fire the pellet at 1440 °C for 5 hr in a zirconia crucible using a horizontal tube furnace with a flowing reducing gas atmosphere (4% H_2/bal. Ar).

2. Exposure, Polishing, and Modification of Ni Mesh Electrode

1. Mechanically grind away one face of the sintered YSZ sample using 6 µm diamond grit until the Ni mesh surface is revealed.

Copyright © 2012 Journal of Visualized Experiments

2. Further polish the exposed Ni mesh surface using 3 µm, 1 µm, and 0.1 µm diamond media in a water / ethylene glycol suspension for approximately 1 min at each polishing step.
3. Ultrasonically clean the polished sample in acetone, ethanol, and DI water for 10 min each.
4. Dry the sample under a clean compressed air stream.
5. For Ni mesh with increased coking resistance, fire the sample at 1,200 °C for 2 hr in reducing atmosphere in the presence of, but not in contact with, BaO powder.

3. Preparation and Electrochemical Testing of Full Cells

1. Brush-paint Ag paste on the opposite surface of the YSZ sample from the Ni-mesh to act as a counter-electrode.
2. Attach a coiled Ag wire to the counter-electrode using Ag paste.
3. After drying the Ag paste on the sample at 120 °C in an oven for 30 min, connect a 0.2-mm diameter Ag wire to the Ni-mesh using Ag paste on the tip.
4. Dry the sample again at 120 °C in an oven for 30 min.
5. Seal the cell (Ni mesh down) on top of a 3/8 inch ceramic cell fixture tube using Aremco Seal 552 (Ceramabond).
6. Allow the sealant to dry in air for 2-4 hr.
7. Connect two insulated silver wires to each of the two electrode wires.
8. Mount the cell fixture in a tubular furnace, connect the fixture to a gas line, and attach the wires to proper electrochemical testing equipment.
9. Begin flowing ultra-high purity grade (99.999%) H_2 gas through the cell fixture at a rate of 50 sccm; the gas should be bubbled through room-temperature water to humidify the gas to 3% vol. H_2O prior to entering the cell fixture.
10. Heat the furnace with the mounted cell to 100 °C for 2 hr, followed by 260 °C for 1 hour, and then finally 800 °C at a ramping rate of 1 °C with continued flowing of H_2 during all heating to avoid oxidation of the Ni electrode. The first two heating steps are for curing the Ceramabond.
11. Hold the cell in the furnace at 800 °C for 2 hr to allow the Ag counter electrode to sinter.
12. Cool the cell slightly to 767 °C for electrochemical performance testing.
13. After testing, carefully remove the cell fixture from the furnace for quenching at room temperature while continuing to flow humidified H_2. (CAUTION: Use proper PPE for handling extremely hot ceramics, such as thermal gloves and mats!)
14. Detach the cell from the fixture for post-characterization by detaching the electrode wires and carefully separating the cell from the Ceramabond sealant.

*__Figure 1__ presents a schematic of the YSZ-embedded Ni mesh cell, along with a typical photograph and optical micrograph of the embedded mesh.

*For our investigations, cells were electrochemically characterized with an EG&G PAR potentiostat (model 273A) coupled with a Solartron 1255 HF frequency response analyzer using CorrWare and ZPlot softwares (Scribner and Associates). Linear sweep voltammetry and constant-voltage amperometry were used to characterize cell performance, and impedance spectra were acquired in the frequency range of 100 kHz to 0.1 Hz with an amplitude of 10 mV. For the sulfur poisoning study, a certified gas mixture of 100 ppm H_2S in H_2 was mixed into the fuel gas stream with pure H_2 to obtain a 20 ppm H_2S/H_2 mixture.

4. Post-test Raman Spectromicroscopic Mapping

1. Affix the cell sample with the mesh anode facing upward onto the Raman microscope stage plate with tape or adhesive to prevent sample movement during Raman analysis.
2. Use the microscope and XYZ stage to locate an interface boundary between the Ni mesh and YSZ substrate.
3. Bring the laser into focus by switching the microscope filters and finely adjusting the Z coordinate of the stage.
4. Set the Raman spectrometer to obtain spectra at the nodes of a rectangular mesh overlaying the area of the interface with 2 µm intervals separating the nodes. The spectra should be centered around the wavenumber(s) corresponding to the Raman mode(s) of the species or phase(s) of interest. In this case, 980 cm^{-1} is chosen for SO_x.
5. For each spectra, integrate the intensity across the Raman mode(s) of interest and divide the intensity by a flat baseline with the same spectrum. The relative intensity can then be plotted in a contour / color map with respect to its coordinates.

Raman spectromicroscopy was performed using a Renishaw RM1000 system equipped with a Modu-Laser StellarPro 514 nm Ar-ion laser (5 mW) and a Thorlabs HRP170 633 nm He-Ne laser (17 mW). The system is equipped with an X-Y-Z motorized stage (Prior Scientific H101RNSW) and a 50X objective lens, which together allow for ~2 µm mapping resolution. Renishaw WiRE 2.0 software was used in conjunction with the hardware. Data was processed using MATLAB (MathWorks).

5. *In situ* Raman Monitoring of Coking[8]

1. Attach an YSZ-embedded Ni mesh sample to the Raman chamber stage using Ag paste with the mesh facing upward.
2. Heat the open chamber to 300 °C for 1 hr to dry and eliminate the Ag paste suspension medium.
3. Seal the Raman chamber's cap and affix it to the Raman microscope stage. Use the microscope to locate a Ni/YSZ interface as described in Protocol 4.2.
4. Begin flowing 4% H_2 / Ar gas humidified by water bubbler through the chamber at ~100 sccm.
5. Heat the Raman chamber to 625 °C.
6. Bring the laser into focus and collect baseline Raman scans from spots on the Ni mesh and YSZ substrate in the 150-2000 cm^{-1} range.
7. Introduce 3-5% C_3H_8 into the gas flow and collect Raman spectra from the Ni at regular intervals while the gas is flowing to observe the deposition of carbon on the surface over time (*e.g.* 15 hr).
8. Cool the sample down slowly (5 °C /min) in flowing 4% H_2 / Ar.

Copyright © 2012 Journal of Visualized Experiments

*The *in situ* Raman analysis was performed with a custom-modified Harrick Scientific high-temperature reaction chamber.The chamber is equipped with a quartz window cap, gas connections, and a cooling line. A schematic and photograph is provided in **Figure 2**.

CAUTION: Cooling water should be used to protect the optical microscope on the Raman system from heating!

6. Nanoscale Visualization of Coking by AFM and EFM

1. Polish one face of a 1 cm x 1 mm square nickel coupon down to the grade of 0.1 µm as described in Protocol 2.2.
2. In a quartz tube-lined furnace, expose the polished nickel coupon to flowing gas containing 10% C_3H_8 balanced by Ar at 550 °C for 1 min; the gas should be bubbled through room-temperature water to humidify the gas to 3% vol. H_2O prior to entering the quartz tube.
3. Remove the sample from the furnace. Inspect the surface morphology by optical microscopy and SEM.
4. Mount the sample onto a metal puck using copper conductive tape for AFM and EFM study.
5. Collect a morphology image using AFM in Tapping Mode.
6. Install an n-type Si based AFM tip (NSC16) or a conductive AFM tip (CSC11/Cr-Au) onto the electrical holder (MMEFCH).
7. Scan the sample surface in "Lift Mode", in which the tip first collects the topographic information on its first trip across the sample surface and then senses the phase angle on its second trip for electrostatic force information. Set the lift height initially to 100 nm, and gradually decrease it to approximately the same value of the surface roughness (20-30 nm).
8. Across a clear interface between the coked and clean region of nickel surface, collect a series of EFM linescans while changing the sample bias.
9. By comparing the EFM linescans at different sample bias potentials, identify the voltage at which the phase angle contrast flips[21].
10. Collect an image with a sample bias that is 1-2V negative w.r.t. the switch point, and another image with sample bias that is 1-2V positive w.r.t. the switch point.
11. By comparing the topography image, and the two sets of EFM images at different sample biases, obtain a distribution map of the carbon and nickel phase on the sample. *For our SPM analyses, a Veeco Nanoscope IIIA system was used. A schematic of the working principle of the EFM analysis[23, 24] is shown in **Figure 3**.

Representative Results

Sulfur Poisoning Analysis

Shown in **Figure 4** are typical I-V and I-P curves of a cell with a Ni mesh electrode under H_2 and 20 ppm H_2S condition. Clearly, the introduction of even just a few ppm of H_2S can poison the Ni-YSZ anode and cause considerable performance degradation.

In order to more intensively understand the poisoning behavior of the Ni-YSZ anode, AC impedance spectroscopy of the cell was performed under open circuit voltage (OCV) conditions. Shown in **Figure 5** are the Nyquist plots for the cell before and after the anode were exposed to fuels containing 0 and 20 ppm H_2S at 767 °C. Two-electrode impedance was used in this study, since the cell impedance is dominated by that of the working electrode; a reference electrode was therefore not needed. The impedance spectra show that the bulk resistance remained the same while the interfacial resistance increased dramatically after the anode was exposed to H_2S-containing fuel.

Shown in **Figure 6** is the typical poisoning and recovery behavior of the cell at 767 °C under 20 ppm H_2S. Both the poisoning and recovery processes seem to finish and reach steady state within a few minutes, which is very different behavior from thick Ni-YSZ anodes that previously studied, where a much longer timeframe was needed especially for the recovery process [25, 26].

Raman intensity mapping was used to gain more chemical information about how the electrode surface interacts with sulfur in fuel gas. **Figure 7** displays an optical micrograph of the Ni/YSZ interface along with a Raman map of the same area plotting the intensity of a mode associated with SO_x species (integrated intensity between 960-1000 cm^{-1}). The species were exclusively observed on the Ni surface and were generally concentrated more away from the TPBs.

In situ Raman Analysis of Coking on YSZ-embedded Ni Mesh

Figure 8a displays an optical micrograph of an unmodified Ni mesh electrode at 625 °C in reducing atmosphere (to prevent undesired Ni oxidation) directly before introduction of C_3H_8. After C_3H_8 began flowing into the chamber, spectra were collected periodically from a spot on the surface of a sample of Ni mesh. This spot is marked by the green circle in **Figure 8b**, which shows the mesh after 15 hr of wet C_3H_8 exposure at 625 °C. Carbon is only detectable on the Ni mesh surface; the spectrum collected from the substrate (red square) shows only YSZ features (**Figure 8c**). A plot of the change in relative carbon signal intensity over the first few hours of exposure time is shown in **Figure 8d**. The intensity of the carbon signal increased as carbon built up on the surface of the Ni from coking. The amount of detectable carbon signal eventually leveled off after a few hours. A Ni mesh sample modified by BaO as described in Protocol 2.5 was subjected to the same experimental conditions. A micrograph of and Raman spectra collected from the surface of the modified mesh sample at the same 15-hour exposure mark as **Figures 8b/8c** are shown in **Figure 8e** and **Figure 8f**, respectively. Carbon signal was not detectable even on the Ni surface in this case.

SPM Analysis of Coking on Ni

Inhomogeneous dark patches formed on the surface of the Ni coupon after it was exposed to C_3H_8-containing gas, which are depicted in the SEM images in **Figure 9**. Shown in **Figure 10** are AFM/EFM images taken from both these light and dark regions.

Copyright © 2012 Journal of Visualized Experiments

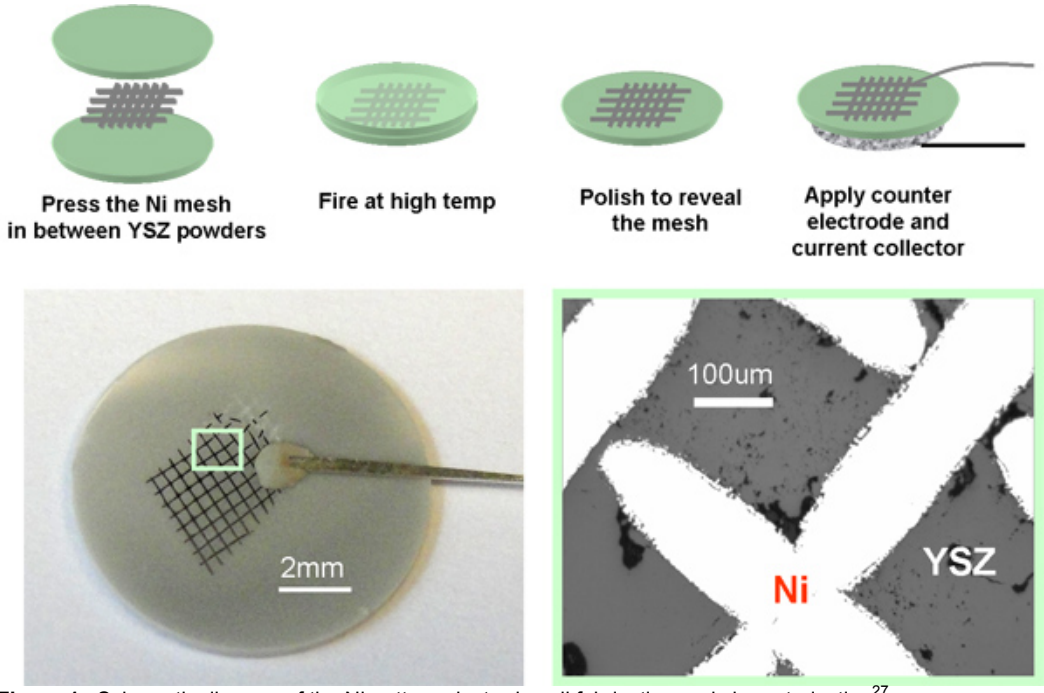

Figure 1. Schematic diagram of the Ni-pattern electrode cell fabrication and characterization[27].

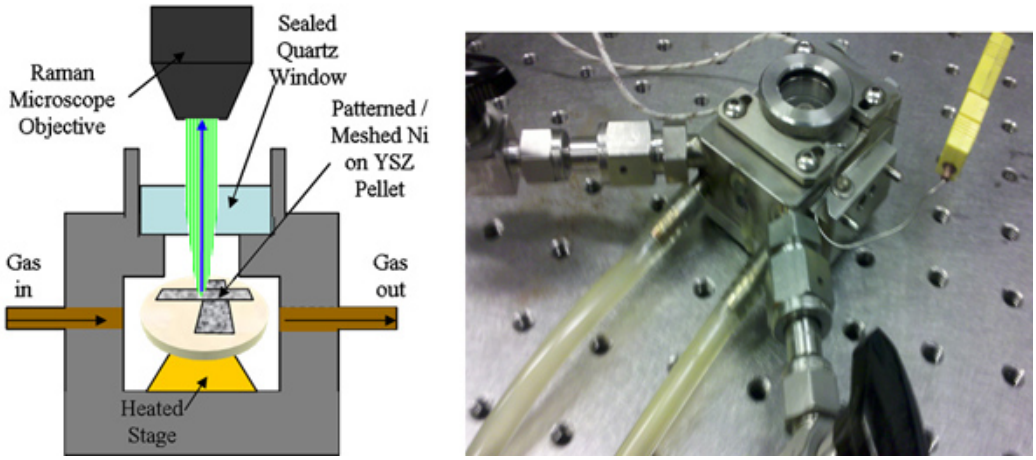

Figure 2. Schematic of environmental chamber setup for *in situ* Raman analysis (left) along with a photograph of the chamber (right). The yellow tubes in the photograph are cooling water lines which are not pictured in the schematic on the left.

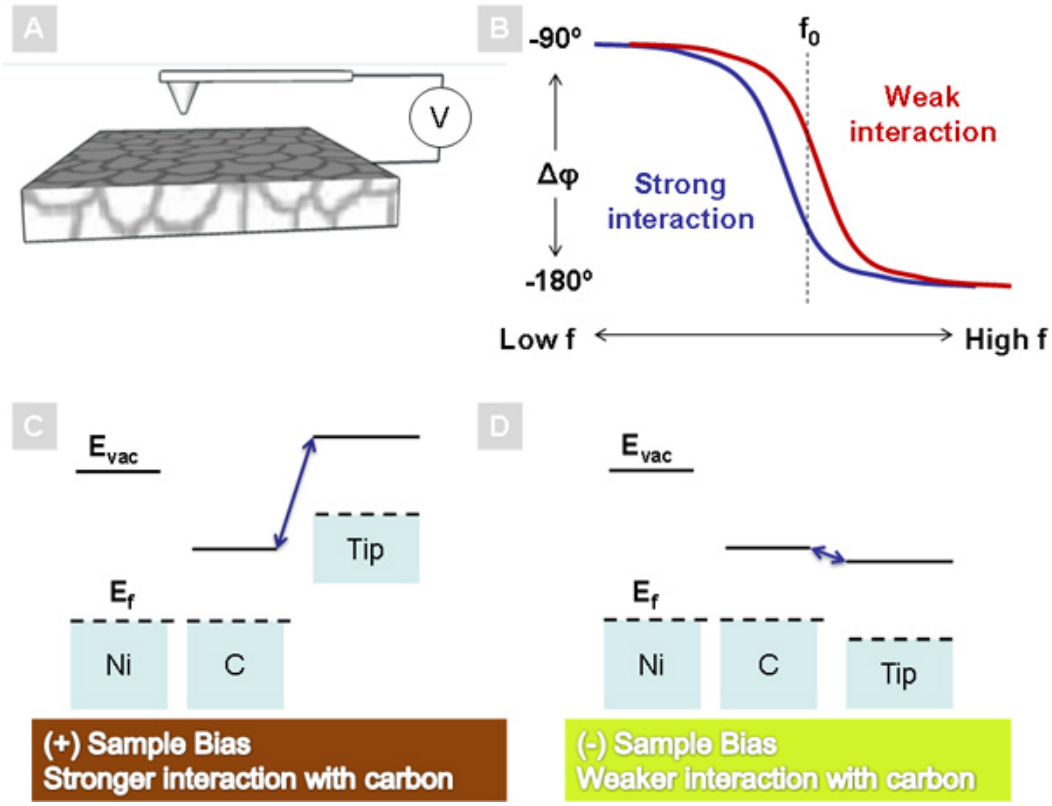

Figure 3. Schematic of the working principle of electrostatic force microscopy (EFM). (A) The schematic showing bias applied onto the sample. (B) The phase angle shift of the AFM tip plot vs. the vibration frequency; strong electrostatic interaction incurs larger degrease in the phase angle. (C) The schematic electron energy band diagram of the sample (nickel and carbon) and tip when the sample is biased positively w.r.t. the tip and (D) when the sample is biased negatively w.r.t. the tip[28].

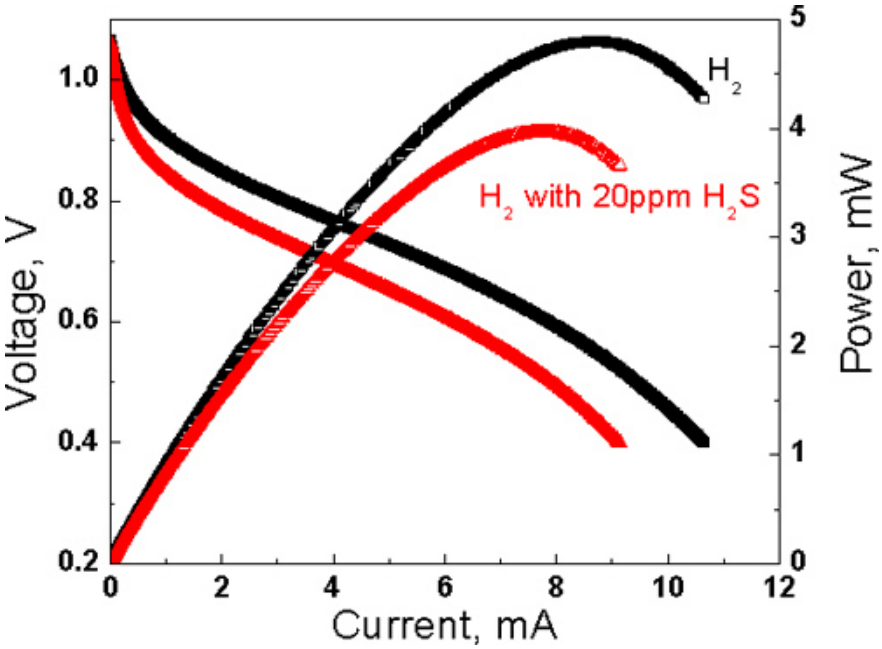

Figure 4. Typical performance of the cell operated under pure H_2 and H_2 with 20 ppm H_2S at 767 °C [27].

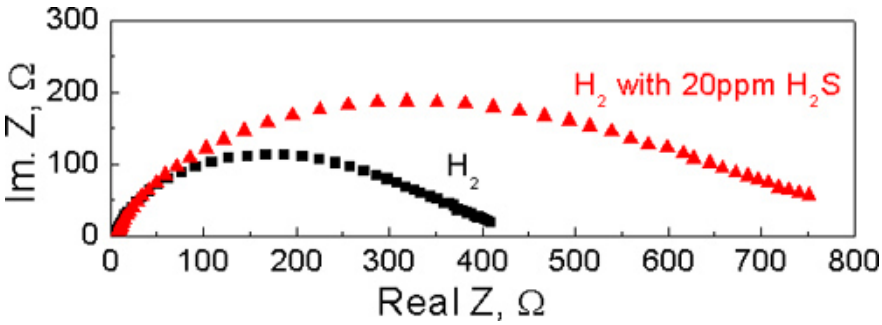

Figure 5. Impedance spectra of the cell with pure H_2 and H_2 with 20 ppm H_2S as fuels measured at 767 °C under open circuit voltage [27].

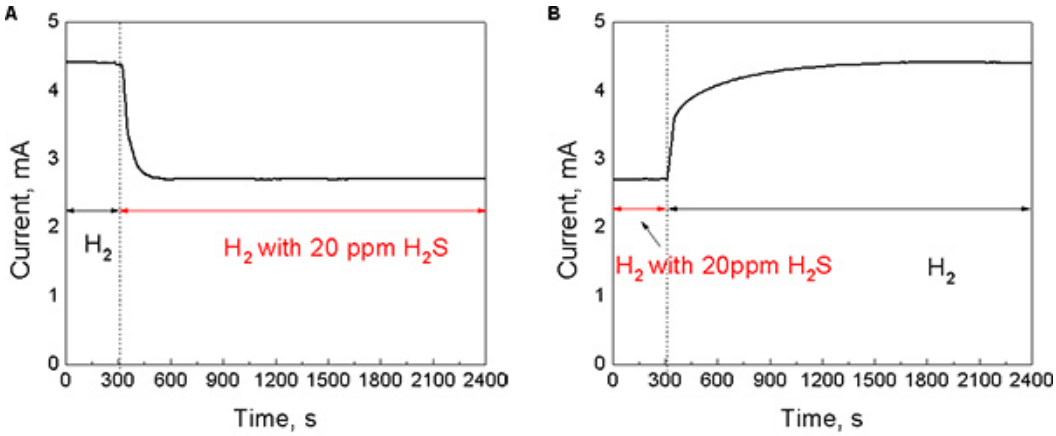

Figure 6. Typical (A) poisoning and (B) recovery behavior of the cell in H_2 with 20 ppm H_2S at 767 °C operated at 0.75V [27].

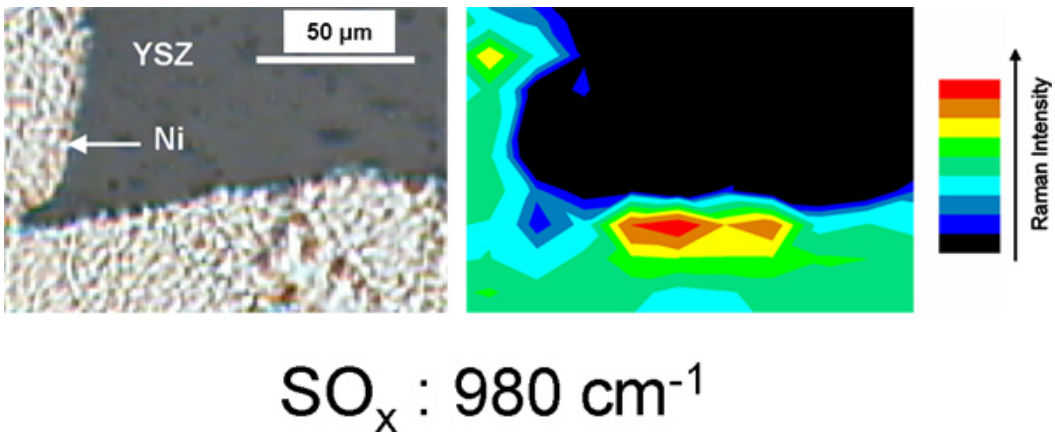

Figure 7. Optical micrograph of corner of patterned Ni mesh electrode in YSZ that was operated in H_2S-containing fuel and aged in air for 18 days (left) along with a Raman map of the SO_x band in the same area (right)[27].

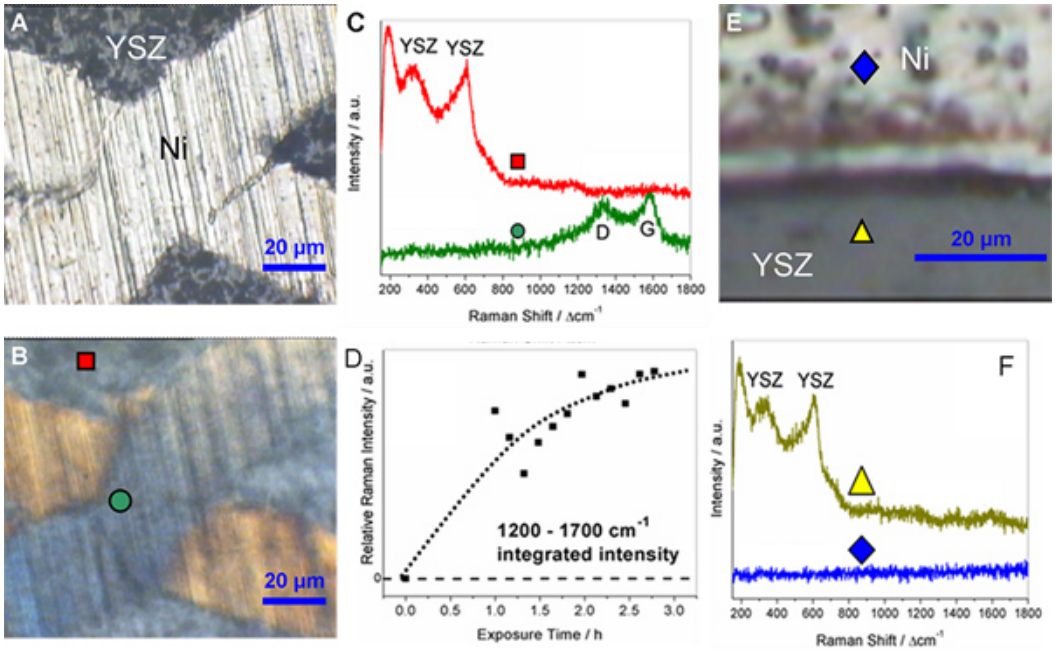

Figure 8. (a) Optical micrograph of Ni mesh embedded in YSZ. **(b)** Same embedded Ni mesh after exposure to C_3H_8-containing gas at 625 °C for 15 hr. **(c)** Raman spectra collected *in situ* from the spots marked in (b) at the 15-hour mark of C_3H_8-containing gas exposure. **(d)** Plot of change in carbon Raman signal intensity collected over time from green circle spot on Ni mesh marked in (b). **(e)** Optical micrograph near interface of BaO-modified Ni mesh and YSZ during the same C_3H_8 treatment. **(f)** Raman spectra collected *in situ* at the 15-hour mark from spots marked in (e). (Reproduced from [8]). Click here to view larger figure.

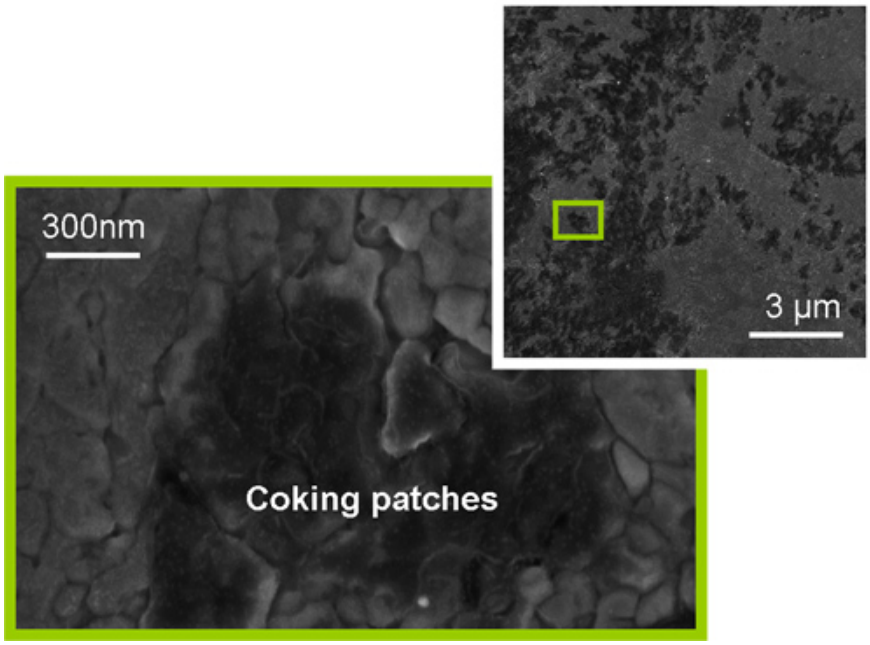

Figure 9. SEM images of coked Ni showing the morphological differences caused by inhomogeneous coking.

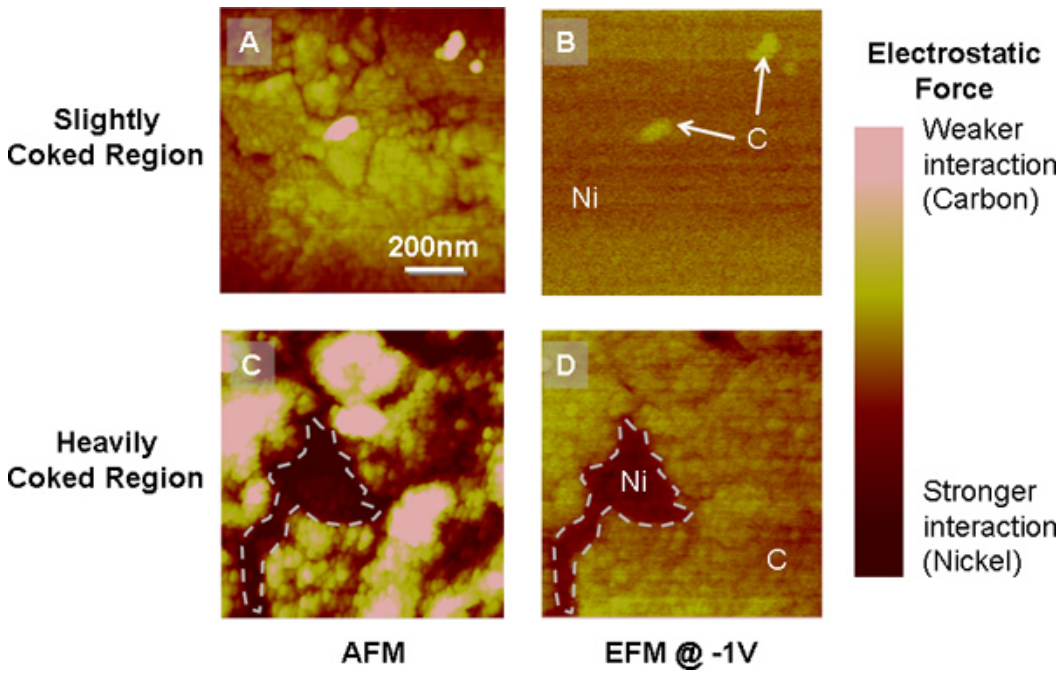

Figure 10. (A) AFM image of the light region shown in **Figure 9** and (B) EFM image of the same area. (C) AFM image of the dark region shown in **Figure 10** and (D) EFM image of the same area. The sample was biased to -1V with respect to the AFM tip, and thus giving a brighter color (weaker tip-sample interaction) to the region covered with carbon.

Discussion

Sulfur Poisoning Analysis

The impedance spectra shown in **Figure 5** suggest that sulfur poisoning is a surface or interfacial phenomenon rather than one that affects the bulk of the material. Specifically, the quick poisoning of the Ni mesh electrode (**Figure 6**) might result from the direct exposure of Ni electrode to the fuel gas and subsequent sulfur adsorption; gas diffusion would not limit the rate of this process as much as in the case of a thick porous Ni/YSZ anode. Strongly adsorbed sulfur at or near the triple phase boundary (TPB) between Ni, YSZ, and fuel would likely block the active sites for electrochemical oxidation of H_2 at the TPB, resulting in quick performance loss. On the other hand, during the recovery process, the current passing through the cell can help the electrochemical oxidation of the sulfur adsorbed on anode surface to SO_2, especially at or near the TPB. Once sulfur is oxidized to SO_2, it will quickly desorb from anode surface, leading to the re-exposure of the Ni/YSZ interface to the gas phase (regeneration of TPBs) and virtually full recovery of the performance [26]. However, the current might not be efficient enough to fully remove the adsorbed sulfur far away from the TPB regions, which may remain on the surface even after full recovery of the performance. This possibility was explored by aging the electrode in air to form SO_x groups that can be detected by Raman spectroscopy (**Figure 7**). The Raman mapping findings support this hypothesis. In addition, no other Ni-S phases could be detected by Raman spectroscopy, which supports the notion that the poisoning process at the studied temperature does not involve new bulk sulfide phase formation.

In situ Raman Analysis of Coking on YSZ-embedded Ni Mesh

The Raman results provide clear evidence that coking occurs preferentially on the Ni surfaces when a Ni-YSZ anode is operated under a hydrocarbon fuel. This preference towards Ni for carbon deposition is likely due to Ni's higher catalytic activity for such reaction over YSZ. On the other hand, carbon deposition was apparently staved off considerably by BaO modification. The modification treatment was similar to the one used in the work done by Yang *et al.* [16], which found that BaO nanoparticles on the Ni surface can stave off coking in the presence of water. The present work supports those findings.

SPM Analysis of Coking on Ni

SEM analysis revealed detailed shape and morphology of the different degrees of carbon deposition (**Figure 9**). The darker patches were likely regions of heavier carbon deposition. Electrostatic force microscopy (EFM) was used in combination with AFM to help confirm this and map the carbon deposition on the nanoscale (< 25 nm resolution). While AFM is capable of distinguishing the morphological variation after hydrocarbon treatment, EFM simultaneously gauges the surface potential through which the surface phases are identified (**Figure 3**). When the sample is biased positively or negatively vs. the tip, the region with lower or higher surface potential (E_{vac}-E_f), respectively, will incur stronger interaction with the tip. Since nickel and carbon, which are the two species present on the sample, each have a different surface potential, EFM is capable of separating them. In the case of our study, the sample was biased to -1 V with respect to the tip, so carbon had weaker interaction with the tip. As shown in **Figure 10**, the light region had less roughness in terms of topography, and only a few spots associated with carbon show up in the EFM image, confirming very light carbon deposition. Meanwhile, the dark region inspected has a great amount of surface roughness, and the majority of the surface is covered by species having weak interaction with the tip, indicating much heavier coking.

Copyright © 2012 Journal of Visualized Experiments

Nanoscale species mapping based on EFM is a promising approach to study the impact of nano-sized catalysts applied onto the materials. For example, by applying BaO onto the nickel surface, the coverage and morphology of coking patches changed drastically. By comparing the EFM images that show the local carbon deposition behavior for different catalysts, their resistance capabilities can be better evaluated.

Disclosures

No conflicts of interest declared.

Acknowledgements

This work was supported by the HeteroFoaM Center, an Energy Frontier Research Center funded by the U.S. Department of Energy, Office of Science, Office of Basic Energy Sciences (BES) under Award Number DE-SC0001061.

References

1. Minh, N.Q. Solid oxide fuel cell technology-features and applications. *Solid State Ionics.* **174**, (1-4), 271 (2004).
2. Liu, M., Lynch, M.E., Blinn, K., Alamgir, F., & Choi, Y. Rational SOFC material design: new advances and tools. *Materials today.* **14**, (11), 534 (2011).
3. Zhan, Z.L. & Barnett, S.A. An octane-fueled solid oxide fuel cell. *Science.* **308**, 844 (2005).
4. Huang, Y.H., Dass, R.I., Xing, Z.L., & Goodenough, J.B. Double perovskites as anode materials for solid oxide fuel cells. *Science.* **312**, 254 (2006).
5. Yang, L., Wang, S., Blinn, K., Liu, M., Liu, Z., Cheng, Z., & Liu, M. Enhanced Sulfur and Coking Tolerance of a Mixed Ion Conductor for SOFCs: BaZr0.1Ce0.7Y0.2-xYbxO3-d. *Science.* **326**, 126 (2009).
6. Liu, M.F., Choi, Y.M., Yang, L., Blinn, K., Qin, W., Liu, P., & Liu, M.L. Direct octane fuel cells: A promising power for transportation. *Nano Energy.* **1**, 448 (2012).
7. Cheng, Z., Wang, J.-H., Choi, Y.M., Yang, L., Lin, M.C., & Liu, M. From Ni-YSZ to sulfur-tolerant anodes for SOFCs: electrochemical behavior, *in situ* characterization, modeling, and future perspectives. *Energy & Environmental Science*. **4**, (11), 4380 (2011).
8. Blinn, K.S., Abernathy, H.W., Li, X., Liu, M.F., & Liu, M. Raman spectroscopic monitoring of carbon deposition on hydrocarbon-fed solid oxide fuel cell anodes. *Energy & Environmental Science*. **5**, 7913 (2012).
9. Abernathy, H.W. Investigations of Gas/Electrode Interactions in Solid Oxide Fuel Cells Using Vibrational Spectroscopy. Ph. D Thesis, Georgia Institute of Technology., (2008).
10. Pomfret, M.B., Owrutsky, J.C., & Walker, R.A. High-temperature Raman spectroscopy of solid oxide fuel cell materials and processes. *Journal of Physical Chemistry B.* **110** (35), 17305 (2006).
11. Cheng, Z. & Liu, M. Characterization of sulfur poisoning of Ni-YSZ anodes for solid oxide fuel cells using *in situ* Raman microspectroscopy. *Solid State Ionics.* **178** (13-14), 925 (2007).
12. Li, X., Blinn, K., Fang, Y., Liu, M., Mahmoud, M.A., Cheng, S., Bottomley, L.A., El-Sayed, M., & Liu, M. Application of surface enhanced Raman spectroscopy to the study of SOFC electrode surfaces. *Physical Chemistry Chemical Physics*. **14**, 5919 (2012).
13. Dresselhaus, M.S., Jorio, A., Hofmann, M., Dresselhaus, G., & Saito, R. Perspectives on Carbon Nanotubes and Graphene Raman Spectroscopy. *Nano Letters.* **10**, 751 (2010).
14. Su, C., Ran, R., Wang, W., & Shao, Z.P. Coke formation and performance of an intermediate-temperature solid oxide fuel cell operating on dimethyl ether fuel. *Journal of Power Sources.* **196**, 1967 (2011).
15. Cheng, Z., Abernathy, H., & Liu, M. Raman Spectroscopy of Nickel Sulfide Ni3S2. *Journal of Physical Chemistry C*. **111** (49), 17997 (2007).
16. Yang, L., Choi, Y., Qin, W., Chen, H., Blinn, K., Liu, M., Liu, P., Bai, J., Tyson, T.A., & Liu, M. Promotion of water-mediated carbon removal bynanostructured barium oxide/nickel interfaces in solid oxide fuel cells. *Nature Communications*. **2**, 357 (2011).
17. Kumar, A., Ciucci, F., Morzovska, A., Kalinin, S., & Jesse, S. Measuring oxygen reduction/evolution reactions on the nanoscale. *Nature Chemistry.* **3**, 707 (2011).
18. Kumar, A., Arruda, T.M., Kim, Y., Ivanov, I.N., Jesse, S., Bark, C.W., Bristowe, N.C., Artacho, E., Littlewood, P. B., Eom, C.B., & Kalinin, S.V. Probing Surface and Bulk Electrochemical Processes on the LaAlO3-SrTiO3 Interface. *ACS Nano.* **6** (5), 3841 (2012).
19. Katsiev, K., Yildiz, B., Balasubramaniam, K., & Salvador, P.A. Electron Tunneling Characteristics on La0.7Sr0.3MnO3 Thin-Film Surfaces at High Temperature. *Applied Physics Letters.* **95** (9), 092106 (2009).
20. Jesse, S., Kumar, A., Arruda, T.M., Kim, Y., Kalinin, S.V., & Ciucci, F. Electrochemical strain microscopy: Probing ionic and electrochemical phenomena in solids at the nanometer level. *MRS Bulletin.* **37**, (7), 651 (2012).
21. Datta, S.S., Strachan, D.R., Mele, E.J., & Johnson, A.T. Surface Layers and Layer Charge Distributions in Few-Layer Graphene Films. *Nano Letters.* **9**, 7 (2009).
22. Coffey, D.C. & Ginger, D.S. Time-resolved electrostatic force microscopy of polymer solar cells. *Nature Materials*. **5** (9), 735 (2006).
23. Nakamura, M. & Yamada, H., Roadmap of Scanning Probe Microscopy. Morita, S. Berlin: Springer (2007).
24. Girard, P. Electrostatic force microscopy: principles and some applications to semiconductors. *Nanotechnology.* **12**, 485 (2001).
25. Rasmussen, J.F.B. & Hagen, A. The effect of H_2S on the performance of Ni-YSZ anodes in solid oxide fuel cells. *Journal of Power Sources.* **191** (2), 534 (2009).
26. Zha, S.W., Cheng, Z., & Liu, M.L. Sulfur poisoning and regeneration of Ni-based anodes in solid oxide fuel cells. *Journal of The Electrochemical Society.* **154** (2), B201 (2007).
27. Liu, M.F., Ding, D., Blinn, K., Li, X., Nie, L., & Liu, M.L. Enhanced performance of LSCF cathode through surface modification. *International Journal of Hydrogen Energy*. **37** (10), 8613 (2012).
28. Park, H., Li, X., Blinn, K.S., Liu, M., Lai, S., Bottomley, L.A., Liu, M., & Park, S. Probing coking resistance from nanoscale: a study of patterned BaO nanorings over nickel surface. In preparation, (2012).

Copyright © 2012 Journal of Visualized Experiments